PAGEOPH, Vol. 143, No. 1/2/3 (1994) 0033–4553/94/030061–27$1.50 + 0.20/0

Simulation of the Frictional Stick-slip Instability

PETER MORA[1] and DAVID PLACE[1]

Abstract—A lattice solid model capable of simulating rock friction, fracture and the associated seismic wave radiation is developed in order to study the origin of the stick-slip instability that is responsible for earthquakes. The model consists of a lattice of interacting particles. In order to study the effect of surface roughness on the frictional behavior of elastic blocks being rubbed past one another, the simplest possible particle interactions were specified corresponding to radially dependent elastic-brittle bonds. The model material can therefore be considered as round elastic grains with negligible friction between their surfaces. Although breaking of the bonds can occur, fracturing energy is not considered. Stick-slip behavior is observed in a numerical experiment involving 2D blocks with rough surfaces being rubbed past one another at a constant rate. Slip is initiated when two interlocking asperities push past one another exciting a slip pulse. The pulse fronts propagate with speeds ranging from the Rayleigh wave speed up to a value between the shear and compressional wave speeds in agreement with field observations and theoretical analyses of mode-II rupture. Slip rates are comparable to seismic rates in the initial part of one slip pulse whose front propagates at the Rayleigh wave speed. However, the slip rate is an order of magnitude higher in the main part of pulses, possibly because of the simplified model description that neglected intrinsic friction and the high rates at which the blocks were driven, or alternatively, uncertainty in slip rates obtained through the inversion of seismograms. Particle trajectories during slip have motions normal to the fault, indicating that the fault surfaces jump apart during the passage of the slip pulse. Normal motion is expected as the asperities on the two surfaces ride over one another. The form of the particle trajectories is similar to those observed in stick-slip experiments involving foam rubber blocks (BRUNE *et al.*, 1993). Additional work is required to determine whether the slip pulses relate to the interface waves proposed by Brune and co-workers to explain the heat-flow paradox and whether they are capable of inducing a significant local reduction in the normal stress. It is hoped that the progressive development of the lattice solid model will lead to realistic simulations of earthquake dynamics and ultimately, provide clues as to whether or not earthquakes are predictable.

Key words: Friction, earthquakes, nonlinear dynamics, lattice solid, numerical simulation, numerical modeling.

Introduction

The nonlinear physics of earthquakes is yet to be well understood despite an extensive research effort. To date, the focus has been on observations and labora-

[1] 4, Place Jussieu, Institut de Physique du Globe, F-75252, Paris, Cedex 05, France.

tory experiments with relatively little theoretical or numerical research. The advent of massively parallel computers marks the beginning of an era when numerical simulations could play an increasing role to resolve questions such as: What are the significant microscopic mechanisms underlying rock friction and how do they work? What are the critical factors controlling earthquakes? Are earthquakes predictable?

Although it may be possible to gain useful insight by ignoring the physics of earthquakes (e.g., analyses based on self-organized criticality and statistics), only a detailed understanding of these phenomena will provide the complete picture. A physically based model would allow numerical experimentation to be performed in order to study: friction, prestress, the effect of rock surface geometry as well as fault geometry, the role of fluids, the development and role of fault gouge, etc. Some well studied models to simulate earthquakes are based on spring-block chains sliding on a frictional surface (e.g., BURRIDGE and KNOPOFF, 1967; CARLSON and LANGER, 1989); integral approaches (e.g., RICE, 1993; COCHARD and MADARIAGA, 1993) and more recently, direct (finite element/difference) methods (DAY, 1991; NIELSEN and TARANTOLA, 1992). These are macroscopically based, and require rather than provide friction laws (for an exception, see PISARENKO and MORA, 1994, who study a mechanism for velocity weakening using a spring-block like asperity model). To our knowledge, no numerical approach has been developed that is capable of accurately modeling the underlying physics of rock friction in order to study the factors controlling the initiation of slip.

The principle goals of this paper are to:

(1) motivate and describe a model with the essential ingredients that enable the physics of rock friction and earthquakes to be simulated at various scales,

(2) present results of a numerical experiment designed to study the friction between two elastic blocks with rough surfaces and *no intrinsic friction.*

Earthquakes are complex phenomena involving processes including friction, fracture, granular flow of fault gouge and wave propagation. They depend on factors such as fault geometry, crustal structure, the state of stress in the crust and the presence of fluids.

The question of how to simulate such diverse processes is not easy considering that scales from the molecular to crustal are involved. A natural and simple approach, termed the "atomic lattice solid" model (MORA and PLACE, 1993), simulates the dynamics of interacting "particles" whose meaning depends on the scale. For example, particles could represent a volume of rock at the crustal scale in which case their interactions describe the macroscopic laws and friction between surfaces, etc. At a smaller scale, particles could represent grains in a rock or molecules in which case studies could be made to develop an improved understanding of the macroscopic laws. Because particles are followed through space, it is easy to model the friction between rubbing surfaces and fracture which involves breaking links between particles as well as elastic wave propagation. At each instant of time, the interactions that occur between nearby particles (e.g., touching or linked)

determine the force on each particle, allowing the particle positions to be extrapolated by a small increment of time. The atomic lattice solid model is based on the same principle as molecular dynamics (ALLEN and TILDESLEY, 1987) except that the interactions are not necessarily interatomic.

The particle based approach is also similar to Lagrangian schemes which follow points attached to matter as they move through space. However, it is computationally easier and physically more natural to model the interactions between particles rather than to compute partial derivatives in an evolving coordinate system that may become convoluted and even discontinuous in the case of fracture processes. Furthermore, the existence of a scale in the problem related to the size of the particles eliminates singularities and infinities that exist in analytic solutions (e.g., Rayleigh poles, caustics, etc.). The requirement of the particle based approach is the specification of the interparticle interactions and any relevant long-range or external forces (e.g., gravitational).

A major part of this paper involves the presentation of simulation results of the friction between two elastic blocks with rough surfaces. The specification of the numerical experiment was in part motivated by laboratory studies involving foam rubber blocks being driven past one another (BRUNE *et al.*, 1990, 1993). Several interesting phenomena were observed including stick-slip cycles with slip histories similar to those recorded at Parkfield California (BAKUN and MCEVILLY, 1984; Fig. 4, BRUNE *et al.*, 1993) and particle motions indicating that the blocks jumped past one another during slip events. BRUNE *et al.* interpreted these motions to be due to interface ("opening") waves of a similar type to those occurring as rubber slides past a hard surface known as Schallamach waves (SCHALLAMACH, 1971). They then suggested that such waves propagating along faults could explain the lack of frictional heat generated during earthquakes (observed along the San Andreas Fault). The idea is that ripples propagate along the fault and that slip occurs while the normal stress is reduced. They also proposed that normal motions related to such opening waves could explain the anomalously high P-wave energy observed beyond the corner frequency.

However, the interpretations of Brune and co-workers are controversial considering the low normal stresses and non rock-like material used in the experiment (foam rubber is highly nonlinear and has a surface geometry that is unlike rock surfaces). In addition, while theoretical work (COMNINOU and DUNDURS, 1977, 1978) indicated that opening waves also occurred when elastic bodies slide past one another, the validity of their solution has been questioned (FREUND, 1978). Furthermore, numerical experiments (DAY, 1991) indicated that the separation component of combined sliding/separation events initiated in a planar fault model rapidly died out. Day suggested that a more complex surface physics or geometry would need to be invoked in order to achieve a self-sustaining separation pulse.

Surface roughness is capable of inducing velocity weakening friction laws both through in-plane dynamical interactions (PISARENKO and MORA, 1994) and the

(steady-state) effect of momentum transfers from the in-plane to normal direction (LOMNITZ-ADLER, 1991). The primary goal of the numerical experiment presented in this paper is to study surface roughness induced friction, and in particular, to investigate the dynamics of slip between rough surfaces involving both normal and in-plane motions. With this in mind and motivated in part by the foam rubber controversy, a numerical experiment was conducted to study the frictional behavior between two perfectly elastic (up to a breaking limit) 2D blocks with rough surfaces. The blocks consisted of particles interacting through radially dependent potential functions thus approximating the behavior of circular frictionless grains. Consequently, the friction between the blocks is entirely due to the effect of surface roughness coupled with the elastic stiffness of the blocks.

The Lattice Solid Model

The "atomic lattice solid model" (MORA and PLACE, 1993) simulates interacting particles that make up a rock (e.g., grains) representing the smallest units of matter in the model. It is similar to the molecular dynamics approach developed in the 1950s to model the motions and interactions of atoms to study the properties of materials (see ALLEN and TILDESLEY, 1987 for a modern review). However, rather than modeling atoms, the dynamics of larger units is simulated. This kind of course-graining of material enables modeling to be performed at geophysical scales on present-day computers which are capable of handling up to 10^8 particles (LOMDAHL *et al.*, 1993a). The principle limitations of the lattice solid model are the validity of course-graining matter into indivisible units and the precision to which interactions between such units can be known. The main strength is that, like the natural universe, the model is made up of interacting particles moving through space. This enables the nonlinear behavior in solids such as friction and fracture to be simulated with considerable simplicity (because rock friction involves surfaces of particles rubbing past one another and fracture involves adjacent particles breaking apart).

Lattice Structure

At the scale of a laboratory experiment to study rock friction, it is appropriate to model particles that represent rock grains. In the present work, idealized round grains defined as particles interacting through radially dependent potential functions are arranged into a close-packed crystalline lattice in 2D (Figure 1). This structure has realistic elastic properties despite being an oversimplification of real rocks which are composed of irregularly shaped grains. The linear elastic properties of the close-packed lattice were first developed by Poisson (AKI and RICHARDS, 1980, p. 4) who demonstrated that it corresponds to an isotropic solid with a

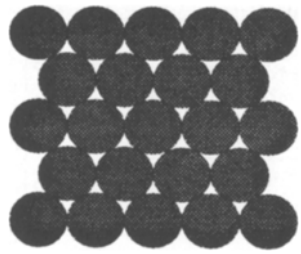

Figure 1
The close-packed 2D lattice used in the lattice solid model.

compressional wave speed $\sqrt{3}$ times the shear wave speed.[2] The disadvantage of the crystalline structure is that the fracture behavior is anisotropic (MORA and PLACE, 1993) whereas fracture in real rocks tends to be isotropic unless grains have a preferred orientation. If isotropy of fracture is an important consideration, a random lattice (i.e., random grain shapes and orientations) should be used (CHRIST *et al.*, 1982; HERRMANN, 1993).

Particle Interaction

Particles interact through interparticle potential functions. To capture the first-order behavior of brittle rocks, the potentials are initially parabolic (i.e., linear elastic bonds) that change irreversibly to a half parabola describing the repulsive component after some critical (breaking) separation r_b is reached (Figure 2). Therefore, bonded particles can essentially be considered to be idealized circular grains that attract one another when pulled apart and repel one another when pushed together. When the bond is broken, the "grains" are free to move apart and collide elastically with any other "grains" in their path. The repulsive part of the interaction remains unchanged after bonds are broken, therefore the "grains" retain their elastic properties when they become free (c.f. an invidividual rock grain has the same elastic properties whether or not it is part of a rock matrix).

Systems of particles with this kind of interaction are capable of modeling dynamic fracturing and frictional behavior in solids (MORA and PLACE, 1993) as well as quasi-static tectonic processes (DONZÉ *et al.*, 1993). Similar reversible potentials have also been used to model fracture at an atomistic level (ASHURST and HOOVER, 1976; LOMDAHL *et al.*, 1993b).

[2] The demonstration assumed interatomic potential functions which were radially dependent only. Note that the ratio $V_p/V_s = \sqrt{3}$ is the same for the 2D and 3D close-packed lattices although the corresponding Poisson's ratios are respectively $\sigma = 1/3$ and $\sigma = 0.25$. Therefore, experiments involving the 2D lattice are equivalent to plane strain experiments involving a 3D solid medium with $\sigma = 0.25$.

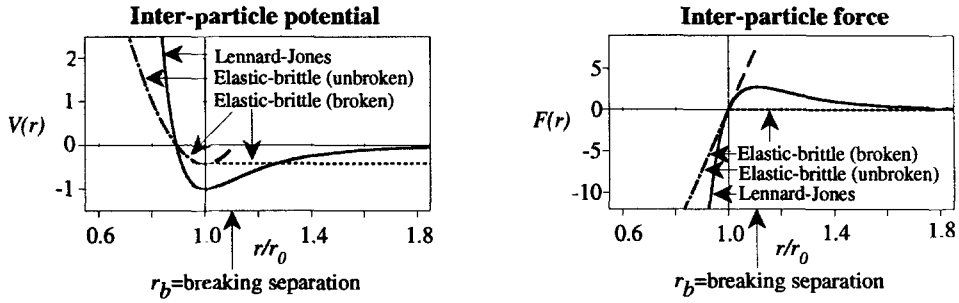

Figure 2
Effective interparticle potentials and corresponding interparticle forces used to model elastic-brittle solids and the Lennard–Jones potential for comparison.

This potential energy function for the elastic-brittle bond described above is given by

$$V(r) = \begin{cases} V_0 + \frac{1}{2}k(r - r_0)^2, & r \le R \\ V(R), & r > R, \end{cases} \tag{1}$$

where the range when the potential becomes flat is

$$R = R(t) = \begin{cases} r_b, & r(\tau) \le r_b \quad \text{for all} \quad \tau < t \\ r_0, & \text{otherwise,} \end{cases} \tag{2}$$

and

$$V_0 = -\frac{1}{2}k(r_b - r_0)^2. \tag{3}$$

The explicit functional dependencies of V and R on time are not written in equation (1) for notational simplicity.

For comparison, the Lennard–Jones potential which is frequently used to approximate the Van der Waals interaction and represents a typical interatomic potential function is

$$V(r) = A\left[\left(\frac{r}{r_0}\right)^{-\alpha} - \frac{\alpha}{\beta}\left(\frac{r}{r_0}\right)^{-\beta}\right], \tag{4}$$

where $\alpha = 12$ and $\beta = 6$ are respectively the powers of the attractive and repulsive parts of the potential. The value of A in equation (4) relates to the spring-constant k through

$$A = \frac{kr_0^2}{\alpha(\alpha - \beta)}. \tag{5}$$

The range when the Lennard–Jones force begins to decrease as a function of the interatomic separation is

$$r_b = r_0\left(\frac{\alpha+1}{\beta+1}\right)^{1/(\alpha-\beta)} \approx r_0\,1.11. \tag{6}$$

At the macroscopic scale, the breaking strain is typically much less than the 11% suggested above due to heterogeneity in chemical composition and lattice defects, etc. Therefore, this value can be considered as an upper bound for most materials.

This limiting value for the breaking separation has been used in the elastic-brittle potential given by equations (1) through (3) because the focus here is on the coupled effect of elastic interactions and surface geometry. Hence, the model material is essentially elastic with breaking occurring only in extreme circumstances.

The total potential energy of an N particle system is the sum of potentials between each unique pair of particles given by

$$V = \sum_{\text{pairs}} V_{nm}^{(2)}, \tag{7}$$

where $V_{nm}^{(2)}$ is the pair potential. Hence, the total interaction force $\mathbf{F}_n^I$ on particle n is given by

$$\mathbf{F}_n^I = -\frac{\partial V}{\partial x_n} = \sum_{m \neq n} \mathbf{F}_{nm}^{(2)}, \tag{8}$$

where x_n is the particle position. The interparticle force on particle n due to particle m denoted by $\mathbf{F}_{nm}^{(2)}$ is given by

$$\mathbf{F}_{nm}^{(2)} = \begin{cases} -k(r-r_0)\mathbf{e}_r, & r \leq R \\ 0, & r > R, \end{cases} \tag{9}$$

where the distance between the particles is

$$r = r_{nm} = |\mathbf{x}_n - \mathbf{x}_m|, \tag{10}$$

and $\mathbf{e}_r$ is the unit vector pointing from particle m to particle n is denoted by

$$\mathbf{e}_r = \frac{\mathbf{x}_n - \mathbf{x}_m}{r}. \tag{11}$$

Equivalent expressions to calculate the torque are unnecessary here, considering that particles have radial interactions only. Note that the absence of torque on individual particles does not exclude torques on groups of particles and thus, torsional waves that may be relevant in cases involving opening surfaces.

It is convenient to introduce viscosity to allow energy to be damped from the closed system. Therefore, the total force on particle n is given by

$$\mathbf{F}_n = \mathbf{F}_n^I - v\dot{\mathbf{x}}_n, \tag{12}$$

leading to a frequency independent attenuation of form $e^{-\alpha t}$ where $\alpha = v/2M_n$ and M_n is the particle mass.

Numerical Solution

Particles are evolved in time by numerical integration of their equations of motion. At time t, the acceleration on each particle is computed using

$$\ddot{\mathbf{x}}_n(t) = \mathbf{F}_n(t)/M_n. \tag{13}$$

The particle positions and velocities are then extrapolated to the next time step $t + \Delta t$, using a finite-difference scheme known as the velocity Verlat scheme (ALLEN and TILDESLEY, 1987) in molecular dynamics literature

$$\mathbf{x}_n(t + \Delta t) = \mathbf{x}_n(t) + \Delta t \dot{\mathbf{x}}_n(t) + \frac{\Delta t^2}{2!} \ddot{\mathbf{x}}_n(t), \tag{14}$$

and

$$\dot{\mathbf{x}}_n(t + \Delta t) = \dot{\mathbf{x}}_n(t) + \Delta t \frac{\ddot{\mathbf{x}}_n(t) + \ddot{\mathbf{x}}_n(t + \Delta t)}{2}. \tag{15}$$

Note that the velocity update requires the acceleration at the next time step. Therefore, the positions at time $t + \Delta t$ are computed first in order to calculate the interaction force and thus acceleration. Due to the viscosity, the total force also requires the velocity at the next time step so a recursion is required. However, the convergence rate is rapid and two iterations were adequate.

The numerical integration was found to be sufficiently precise using a time step Δt

$$\Delta t \leq \varepsilon \frac{r_0}{V_{\max}}, \tag{16}$$

where $\varepsilon \approx 0.2$ (denoted the numerical integration precision factor) and $V_{\max} = V_p$ where V_p is the compressional wave speed and corresponds to the maximum speed of information propagation in the numerical experiment defined in the following section.

Lattice Solid Properties

Since the time of Poisson and Cauchy, it has been known that a close-packed 2D lattice has isotropic elastic properties in the macroscopic limit with a compressional to shear wave speed of $\sqrt{3}$ (i.e., $\lambda = \mu$). Therefore, in the long wavelength limit, the shear wave speed V_s relative to the compressional wave speed V_p is

$$V_s = \frac{V_p}{\sqrt{3}} \approx 0.58 V_p, \tag{17}$$

and the Rayleigh wave speed V_R is

$$V_R \approx 0.92 V_s \approx 0.53 V_p, \tag{18}$$

which are typical ratios for crustal rocks. Because the medium is made of discrete particles, the wave speeds are a function of wavelength and may be significantly different as the wavelength approaches the equilibrium separation between particles. Note that real materials such as rocks have similar behavior at small scales (e.g., molecular or granular). Consequently, this dispersive behavior is not considered to be a fundamental limitation in the sense that both the model and rocks have certain behavior controlled at the smallest scale. However, the range between the seismic and "smallest scale" in the real world is high (e.g., between 10^6 = km/mm and 10^{12} = km/nano-m) whereas the maximum range possible on today's most powerful computers is 10^4 in 2D problems (i.e., 10^8 particles). Consequently, the role of the lattice solid discreteness must be carefully considered when interpreting the simulation results in terms of earthquake dynamics.

The macroscopic elastic moduli are related to the microscopic parameters (i.e., the spring constant k and equilibrium separation r_0) by

$$\lambda = \mu = \frac{\sqrt{3}}{4} k, \tag{19}$$

(HOOVER *et al.*, 1974) and (area) density

$$\rho = \frac{2}{\sqrt{3} r_0^2} M. \tag{20}$$

Numerical Experiment

Two-dimensional homogeneous elastic-brittle blocks with crudely defined rough surfaces were rubbed past one another at a constant rate as shown in Figure 3. Each block consisted of approximately 256 × 128 particles attached to a rigid driving plate on the outer edge. The driving plates were maintained at a given separation corresponding to an initial deformation of 1%, suggesting a normal stress of order 10 Kbars.[3]

The model size was insufficient to enable the specification of a realistic rock surface roughness (e.g., BROWN and SCHOLZ, 1985) and this should be recalled when interpreting the results. The rough surfaces of the blocks were initialized by deleting (etching) particles from the edge of a flat block that lay outside a function with a power-law spatial spectrum of heights. This function was generated by

[3] The equivalent normal stress was calculated for $V_p = 5$ km/s and $\rho = 3$ gm/cm^3.

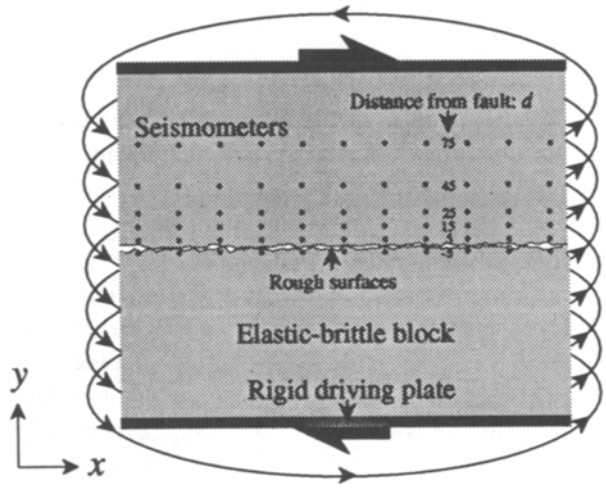

Figure 3
The setup of the numerical friction experiment. The distance from the fault is given in terms of the separation between rows of particles. Positive and negative signs are respectively used to indicate seismometer rows above and below the fault.

multiplying independent white noise with $k_x^{-\gamma}$ and inverse Fourier transforming. Its height range was equal to three times the distance $\Delta y = (\sqrt{3}/2)r_0$ between rows of particles (i.e., approximately 1% of the total model height). Therefore, the surface roughness can be considered to have three possible discrete values ranging from the minimum value[4] of $(1-\sqrt{3}/2)r_0$ to the maximum in increments of Δy. A value of $\gamma = 0.5$ corresponding to pink noise (SCHROEDER, 1991) generated a reasonable surface roughness given the limited model size.

The particle mass M, spring constant k and equilibrium separation of particles r_0 were all set to unity in the numerical experiment and a time step of $\Delta t = 0.2$ was used, corresponding to a numerical integration precision factor of $\varepsilon \approx 0.2$. In this system of units, the compressional wave speed (see equations (19) and (20)) is

$$V_p = \sqrt{\frac{\lambda + 2\mu}{\rho}} = \sqrt{\frac{9}{8}}\frac{1}{r_0}\sqrt{\frac{k}{M}} \approx 1.06 \sim 1. \tag{21}$$

[4]The minimum surface roughness is not zero considering the smoothest surface that can be defined using the lattice solid model is a row of particles (see Figure 1). It is calculated as the difference between the row spacing and particle diameter which is the normal movement required for a free particle to move along a "smooth" surface (i.e., a row) while touching the surface.

Hence, from equations (17) and (18), the shear and Rayleigh wave speeds are respectively

$$V_s \approx 0.61, \tag{22}$$

and

$$V_R \approx 0.56. \tag{23}$$

Other systems of units can be obtained by choosing V_p in the desired system and rescaling.

The particle diameter r_0 determines the scale of the model and in particular, the minimum asperity size and seismic wavelength that can be represented. Together with the numerical integration precision factor ε, r_0 and V_p determine the time step Δt and therefore, the time scale (see equation (16)). For example, with $V_p = 5$ km/s and $r_0 = 100$ m, the model size and time step would respectively be $25.6 \times (22.6\sqrt{3}/2) \approx 25.6 \times 22.2$ km^2 and $\Delta t \approx 0.004$ *s*.

Circular boundary conditions were used in the x direction and the rigid plates were driven at a constant speed of 0.00025 (i.e., approximately 0.025% of the compressional wave speed) representing the steady movement of tectonic plates. Computations were made for 100,000 time steps = 20,000 units of time on a massively parallel Connection Machine[5] of the C.N.C.P.S.T.[6] The particle velocities were initially zero adjacent to the fault and varied linearly to the "tectonic" values at the rigid driving plates. A uniform shear deformation equivalent to 1,000 units of time was applied to decrease the length of the period prior to the first slip event (i.e., the blocks were initially sheared by the amount that would be achieved after 1,000 units of time if there was no slip between the rough surfaces).

A value for the viscosity of $\nu = 0.016$ was used to attenuate elastic energy released in simulated earthquakes in order to decrease the effect of boundary reflections on the dynamics of the frictional process along the fault. Hence, the attenuation coefficient was $\alpha = 2\nu/M = 0.008$ and waves were attenuated according to $e^{-0.008T}$ where $T = S/V$ is the time taken for a wave to propagate a distance S at a speed V. Therefore, boundary reflections from the rigid driving plates of shear and compressional waves generated along the fault[7] were respectively attenuated by factors of $e^{-2.88} \approx 0.056$ and $e^{-1.66} \approx 0.19$ in addition to the geometrical spreading factor. The artificial attenuation is intended to emulate the combined effect of

---

[5] A 64 node partition of a 128 node CM-5. The Connection Machine© is produced by Thinking Machines Corporation, Cambridge, MA, U.S.A.

[6] Centre National de Calcul Parallèle en Sciences de la Terre, Institut de Physique du Globe, Paris, France.

[7] Note that the vertical propagation distance from the fault to the rigid driving plates and back to the fault again is $S = 0.99 \times 256 \times \Delta y \approx 219.5$.

physical attenuation and geometric spreading on real seismic radiation as it propagates around the globe, thereby having little effect on the future dynamics at the fault of origin. Without the viscosity, normal modes of the system periodically initiated slip along the fault, making it difficult to observe stick-slip cycles.

Seismometers were located on the upper and lower blocks to measure the displacement, velocity and acceleration along rows of particles at various distances from the fault (Figure 3) measured in terms of the row separation, $\Delta y = (\sqrt{3}/2)r_0$.

Stick-slip Cycles

Figure 4 depicts the frictional force, defined as the difference in the horizontal component of force on the upper and lower driving plates,

$$F = \sum_{n \in \text{lower edge}} (F_x)_n - \sum_{n \in \text{upper edge}} (F_x)_n. \tag{24}$$

Stick-slip cycles can be seen as the characteristic sawtooth shapes observed in laboratory experiments (e.g., in experiments involving rubbing metal against metal (BOWDEN and TABOR, 1950), paper against paper (HESLOT *et al.*, 1994) and rocks against rocks (BYERLEE and BRACE, 1968; see also DIETERICH, 1978 who analyzed sawtooth tips in rock friction experiments to study preseismic slip). During the stick phase, asperities on each surface lock the blocks together and the force gradually builds up as the blocks deform. Eventually, the elastic stress in the medium is sufficient to push a given asperity on one surface past its partner on the other surface, initiating slip between the blocks. Note that prior to 5,000 units of time, the force increases on average as the system is loaded to the critical point.

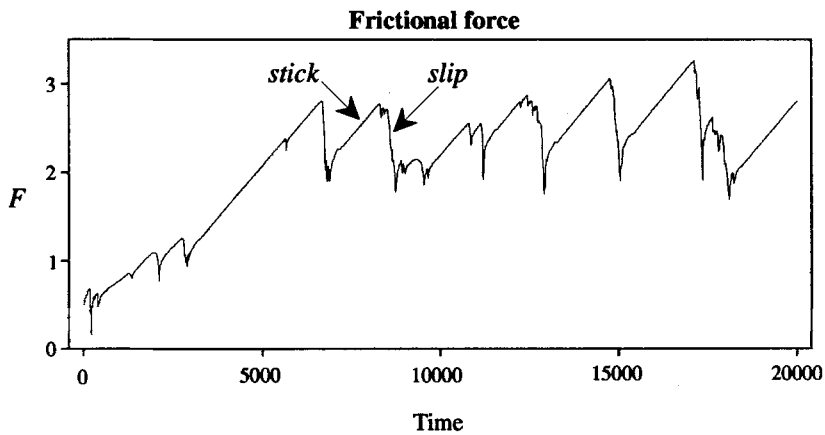

Figure 4
The frictional force as a function of time between two elastic-brittle blocks with rough surfaces rubbing past one another. The sawtooth shapes are stick-slip cycles.

Subsequently, the force oscillates around a constant value during the stick-slip cycles.

During the slip phases, elastic energy is radiated into the blocks as the surfaces rub past one another as can be seen on Figure 5 depicting the acceleration at a distance of $d = 15$ rows from the fault (see also Figure 13). During the stick phases, no significant energy can be seen in the accelerograms (i.e., these are quite periods between the dominant earthquakes).

During the slip phases, the two sides of the fault rapidly move past one another leading to step-like shapes in the displacement recordings (Figure 6). The steps are often sharp, indicating that movement tends to occur during short periods. However, at certain positions along the fault, steps are smooth or subdivided into smaller steps, indicating that the movement can also occur continuously over a longer period (c.f. aseismic slip) or as a series of small stick-slip events. It is interesting that in places, only a part of the fault breaks such as at $t \approx 11{,}000$. In these cases, the rupture has stopped spontaneously, probably upon reaching a larger than average asperity (i.e., higher than average local normal stress).

Figure 7 displays an accelerogram adjacent to a displacement curve where eight stick-slip cycles have been identified. These recordings are remarkably similar to laboratory measurements involving stick-slip between foam rubber blocks (BRUNE *et al.*, 1990) and the displacement curve has a similar form as field measurements from Parkfield (BAKUN and MCEVILLY, 1984). Despite the relatively high rate the blocks were rubbed past one another ($0.00025V_p \sim$ m/s) as compared with tectonic values ($\sim$cm/yr) or laboratory rates ($\sim \mu$m/s $\sim$ cm/day), the stick-slip process is well modeled.

Figure 7 shows that the amount of displacement during each slip event is a half unit. Consequently, the total relative displacement between the two sides of the fault is one unit (i.e., a particle diameter), implying that each slip event involves a

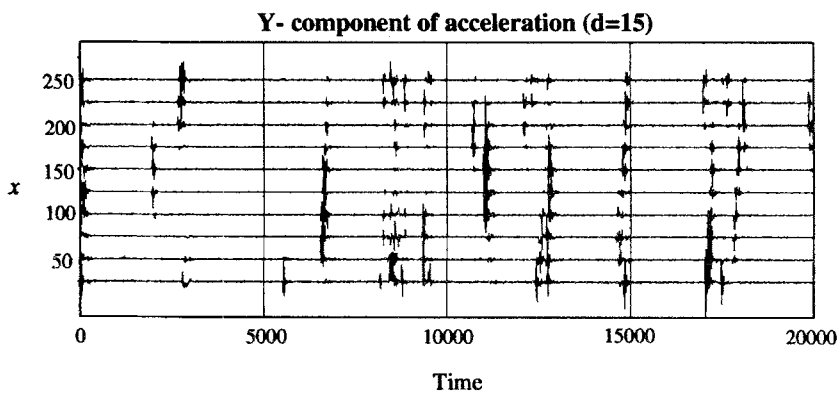

Figure 5
Seismograms of the y component of acceleration.

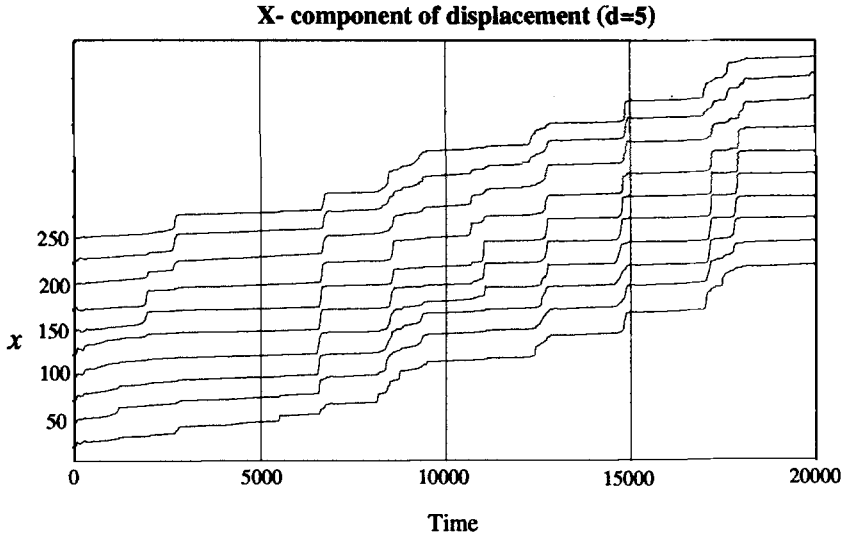

Figure 6
Seismograms measuring the x component of displacement at a distance of $d = 5$ rows from the fault. The slip phases are seen as steps in the curves.

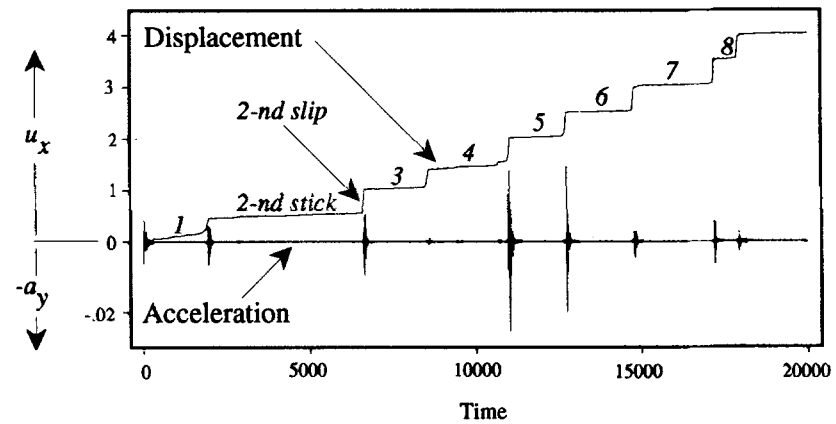

Figure 7
Seismograms recording the x component of displacement and the y component of acceleration at position $x = 150$ and a distance $d = 5$ rows from the fault.

particle on one surface sliding past its counterpart on the other surface. However, the complex nature of the steps seen in Figure 6 indicates that this is only true on average. The complexity is due to the surface roughness and is expected to become increasingly rich with model size when more realistic surfaces could be specified. Apparently, the main effect of the roughness was to make the stress heterogeneous but it was too crude to allow a greater variability of slip magnitude to occur.

Note that the second and sixth slip phases are the least complex (see Figures 4 and 6) and these periods will be analyzed in greater detail.

Typical seismograms measuring acceleration during the second and sixth slip phases are shown in greater detail in Figure 8. It is not easy to compare these with observed seismograms because they are recorded in the near field (i.e., at a distance that is less than the length of the rupture zone).

Spectra

The average amplitude spectrum of the x and y components of acceleration have been computed in Figure 9. Both spectra are approximately linear (on the log–log plot) within a given range with the slope of the y-component spectrum changing at a lower corner frequency related to the fault size. These features are qualitatively similar to observed and theoretical spectra. Theoretical models predict that in the far field (and in 3D), the amplitude spectrum of acceleration will be flat above the corner frequency and have a slope of 2 below the corner frequency (AKI and RICHARDS, 1980, pp. 823–825). The numerical spectra have a slope of approxi-

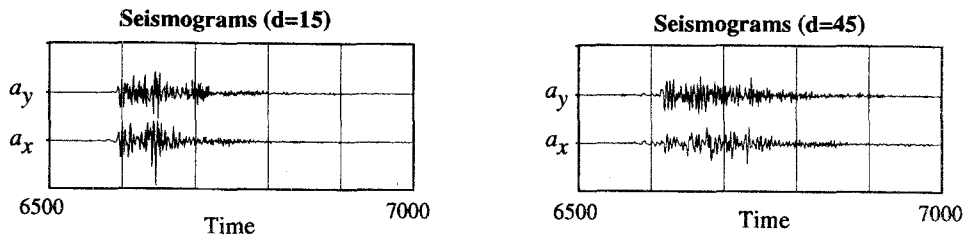

Figure 8
Typical seismogram recordings during the second slip event showing the x and y component of acceleration. The seismometers were located at $x = 150$ with respective distances from the fault of $d = 15$ and $d = 45$.

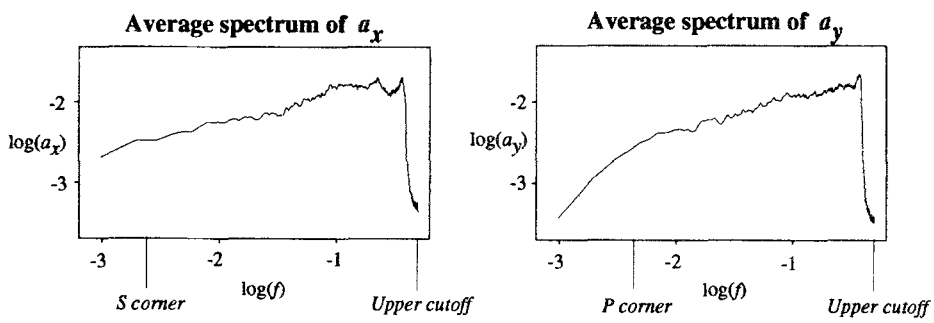

Figure 9
Average amplitude spectra of acceleration.

mately 0.4 above the corner frequency and 1.5 below the corner frequency in the case of the y-component spectrum. The x-component spectrum does not have a clear change of slope at the corner frequency. Departures from observed and theoretical spectra are probably due to the fact that the numerical results are 2D and seismometers were located in the near field. This interpretation is supported by the observation that the numerical spectra become increasingly flat at high frequencies.[8]

Note that the corner frequencies marked on the plots were calculated using

$$f^P_{\text{corner}} = \frac{V_P}{L},$$

and

$$f^S_{\text{corner}} = \frac{V_S}{L},$$

where L is the length of the fault.

The spectra also exhibit an upper frequency cutoff related to the finite particle size computed as

$$f^P_{\text{cutoff}} = \frac{V_P}{\lambda_{\min}} = \frac{V_P}{(2r_0)},$$

which is the frequency of shortest wavelength P waves.

Rupture Velocity

The y component of particle velocity during the second and sixth slip phases is shown in Figure 10. The speed of the rupture front can be obtained by measuring the slope of the onset of the first black events yielding a value $V_r \approx 1.2V_s$ during the second slip phase and $V_r \approx V_R$ during the sixth slip phase. During the other slip phases, rupture speeds had values close to the above two values with the majority (3 of 5 measured) close to the Rayleigh wave speed and the remainder close to $1.2V_s$ (i.e., between the compressional and shear wave speeds). By comparison, phase velocities of Comninou and Dundurs elastic interface waves between elastic media (COMNINOU and DUNDURS, 1977, 1978) lie between the shear and Rayleigh wave speeds.

However, the observation of some rupture speeds above the Rayleigh wave speed and even above the shear wave speed is in agreement with numerical modeling results, theoretical analyses and field observations. In particular,

[8] Higher frequence ⇒ shorter wavelength ⇒ far field approached.

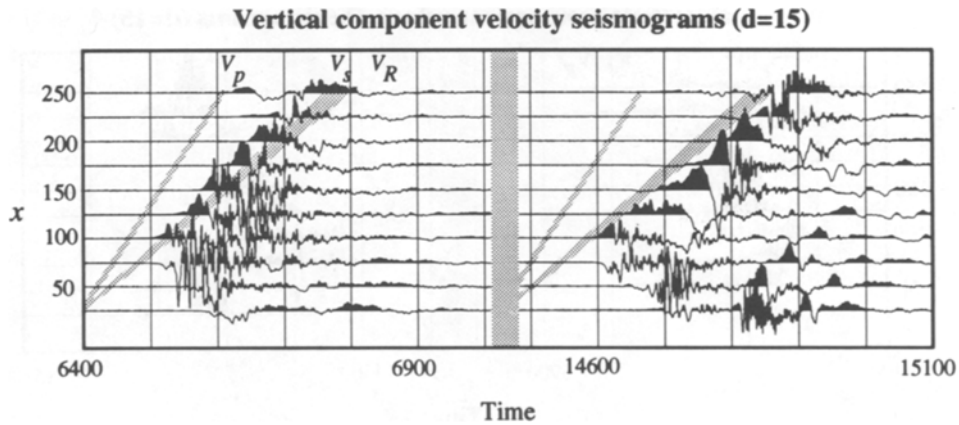

Figure 10
Seismograms of the y component of particle velocity with one trace width representing 0.5% V_p. The diagonal grey lines indicate the slopes corresponding to the compressional, shear and Rayleigh wave speeds.

ANDREWS (1976) numerical modeling results suggested that a secondary fracture could be induced ahead of the main crack tip, precipitating crack growth at a speed beyond the Rayleigh wave speed. BURRIDGE *et al.* (1979) explained under what conditions shear cracks could propagate at speeds between the shear and compressional wave speeds. An interpretation of the Imperial Valley earthquake suggests that the boundary of a slip zone may propagate at speeds above the shear wave speed in crustal rocks (ARCHULETA, 1982).

Slip Pulses

The x component of particle velocity during the second and sixth slip phases is shown in Figure 11 with one trace width representing 1% of V_p (c.f. one trace width on Figure 10 represented 0.5% of V_p). These plots indicate that slip occurs as a pulse that propagates along the fault in a similar manner to HEATON's (1990) self-healing slip pulses. The x- and y-component particle velocity seismograms for the sixth slip event suggest that the slip can be decomposed into two parts: (1) a low slip rate initial phase whose front propagates at the Rayleigh wave speed and; (2) a high slip rate main pulse which grows from the initial phase and whose front propagates at a speed well above the shear wave speed. It is interesting to note that the peak of the main pulse propagates at a speed approaching the compressional wave speed.

The horizontal particle velocities range up to a few percent of the compressional wave speed (~ 100 m/s) during a slip event. The logarithmically averaged horizontal particle velocity in the main pulse of the second and sixth slip events is approxi-

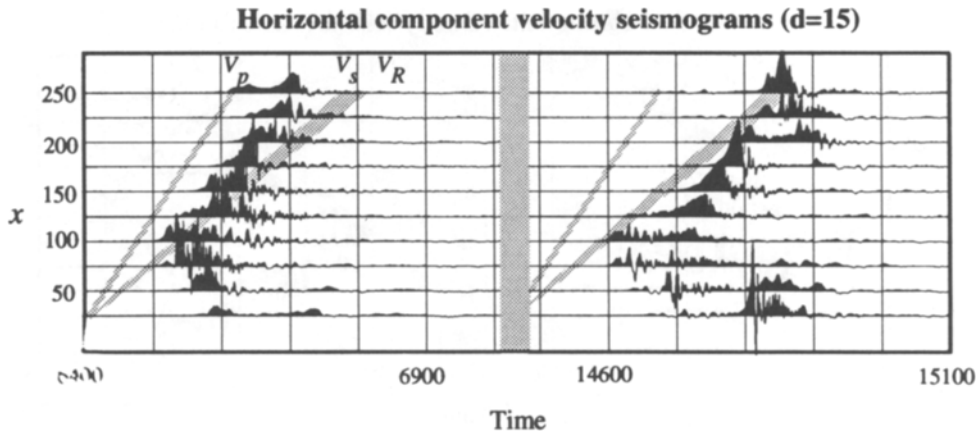

Figure 11
Seismograms of the x component of particle velocity with one trace width representing 1% V_p. The diagonal grey lines indicate the slopes corresponding to the compressional, shear and Rayleigh wave speeds.

mately 0.3% of V_p (i.e., 15 m/s assuming $V_p = 5$ km/s). In the initial low slip rate part of the pulse of the sixth slip event, the maximum horizontal particle velocity is 0.5% V_p (25 m/s) and the logarithmically averaged value is 0.05% V_p (2.5 m/s).

By comparison, Heaton estimated logarithmically averaged particle velocities during a slip pulse to be ~ 1 m/s (HEATON, 1990) and suggested that the maximum particle velocities could be as high as 10–20 m/s. The numerical particle velocities are approximately a factor of 5–15 higher than these values in the main part of the pulse and are similar in magnitude in the initial low slip rate part of the sixth slip event that propagates at the Rayleigh speed.

If Heaton's values are representative of particle velocities extremely close to a fault, it seems probable that the mechanics and behavior of initial low slip rate parts of simulated pulses are most relevant to real earthquakes. It should be noted that the speed of the rigid driving plates was high, namely 0.00025 $V_p = 1.25$ m/s (assuming $V_p = 5$ km/s) which is comparable to Heaton's slip rates. Consequently, the fault is being driven closer to instability even during a slip event. This suggests that progressively smaller elastic perturbations may be capable of destabilizing the fault surfaces and initiating slip (e.g., those associated with a compressional wave) which may help to explain the higher speed main pulses observed in the numerical experiment. In other words, the high speeds of the rigid driving plates may favor a different slip mechanism in the main pulse than the mechanism that occurs during real earthquakes.

It should be noted that Heaton considers his 1990 particle velocity estimates to be lower bounds for particle velocities near a fault where the pulse could be more peaked (HEATON, 1994). Therefore, on the basis of particle velocities alone, it

should not be excluded that the main part of the simulated pulse is relevant to earthquakes and would be observed should there be a sufficient number of seismometer recordings near a fault to simultaneously estimate both the slip form and rate.

In summary, the possible reasons for the high particle velocities within the main pulse relative to values obtained through seismogram inversion are:

(1) simplification in the model such as the lack of intrinsic friction between particles,
(2) uncertainty in the estimates based on analyses of real seismograms due to data errors and false assumptions regarding the form of the slip pulse etc., and
(3) difficulty in making comparisons between the numerical particle velocities measured adjacent to the fault and inverted values using seismograms that are typically less close to the slip zone.

The first possibility will be investigated in the future, by conducting numerical simulation studies using less simplified particle interactions that include friction between particles. The second and third possibilities could perhaps be investigated by reanalyzing a data set containing only seismograms that are extremely close to the slip zone to determine whether there is any evidence for rapidly propagating high slip rate pulses like those seen in the numerical experiment.

Particle Motions

Particle trajectories at four different distances from the fault are shown in Figure 12, with a circle plotted every 10 units of time. The particle trajectory plots show that there are significant normal motions and that the upper and lower fault surfaces seem to jump apart when the slip occurs.

The particle trajectories five rows above the fault are similar to those observed by BRUNE *et al.* (1993) which led them to suggest that opening waves may occur during earthquakes, which could explain the heat flow paradox. It is therefore interesting to analyze the magnitude of the normal particle motions.

Recall that each slip event increased the average relative displacement across the fault by one particle diameter. This means that despite the surface roughness, the slip involves particles on one surface slipping past their counterparts on the other surface and no slip between larger asperities. Normal motions that separate the blocks by an amount approximately equal to the difference between the particle diameter and row separation (i.e., $1-\sqrt{3}/2 \approx 0.13$) would allow this to occur without any stress change (i.e., the normal motion required for touching rows to ride over one another without penetration or separation).

The normal motions recorded on the upper and lower blocks (i.e., at $d = 5$ and $d = -5$) indicate that the separation during slip ranges up to approximately 0.2 units, suggesting that the fault surfaces may slip with a reduced stress in some instances. Unfortunately, the current results are not capable of resolving whether

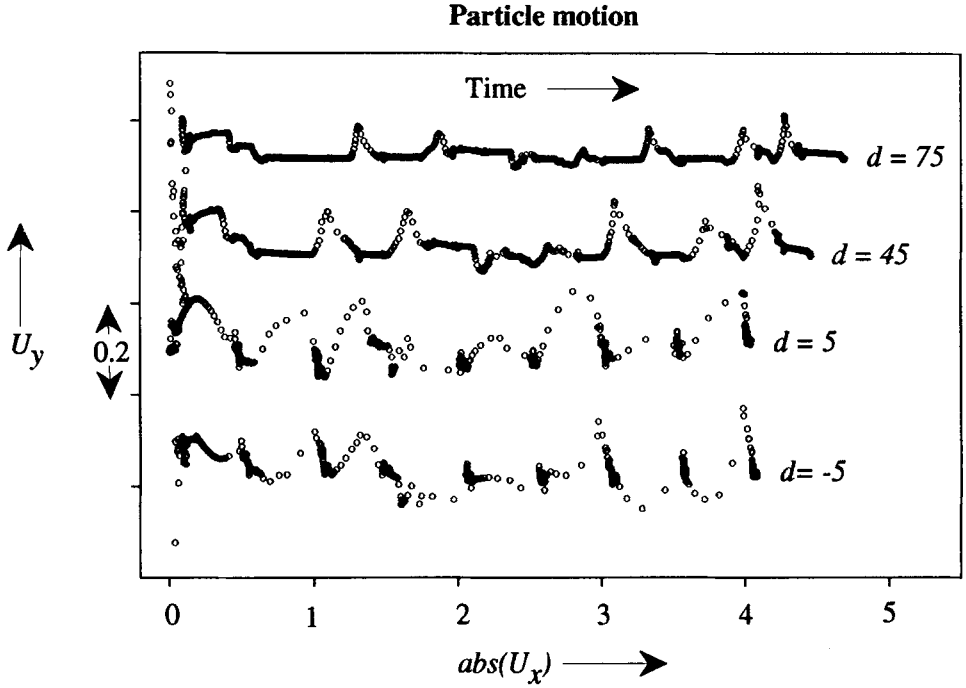

Figure 12
Particle trajectories recorded by seismometers located at four distances from the fault at $x = 150$. The absolute value of the horizontal displacement is plotted to facilitate the comparison between trajectories on the upper and lower blocks. Note that the horizontal displacements recorded on the lower block at $d = -5$ were negative.

the normal stress drops on average. This would require surface data to be collected and analyzed which is beyond the scope of the current paper whose primary goals are to describe the model and present results of a numerical experiment designed to study friction.

Snapshots

Snapshots during the 6th slip phase are shown in Figure 13. Initially the blocks stick together as asperities on either side of the fault interlock. Eventually, stress builds up sufficiently for a given pair of asperities to slide past one another (first

Figure 13
Snapshots of a synthetic earthquake event occurring during the 6th slip of the 2D numerical friction experiment. Colors representing the vertical component of particle velocity are superimposed on an artificial landscape containing mountains and geologic layers. This allows the displacement across the fault to be seen at the same time as the particle velocities.

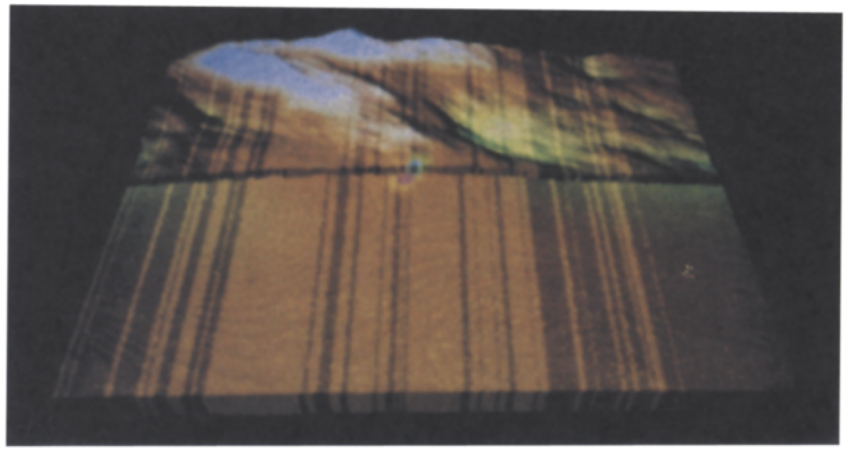

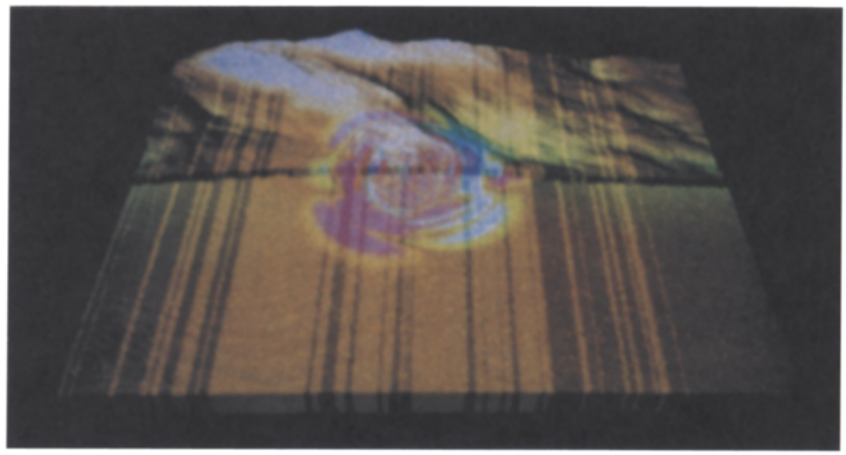

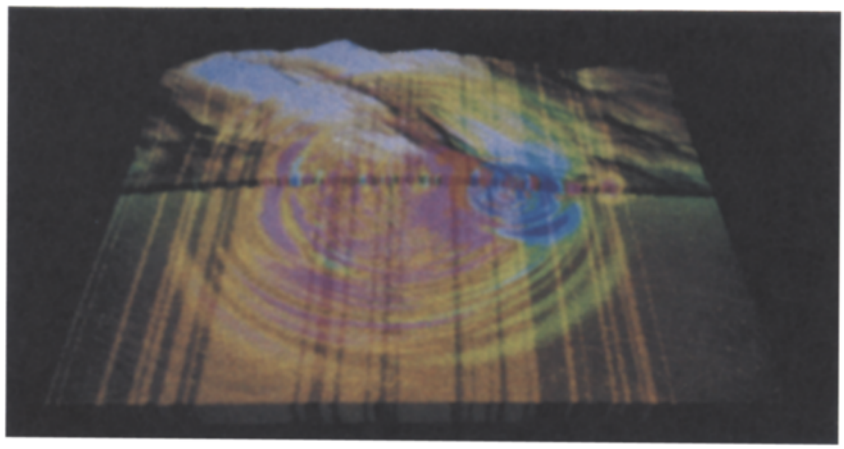

image). This radiates waves into the medium and excites a slip pulse that propagates along the fault, leaving a wake of interface waves behind it whose magnitude rapidly decays with distance from the fault. Note that the epicenter was centered graphically in Figure 13 by applying the appropriate circular shift to the display fields in the x direction.

Discussion

The numerical results indicate that a slip pulse involving normal motions can be sustained provided surface roughness is present as suggested by DAY (1991). It is not clear whether it is the surface roughness alone that induces the normal motions or whether they relate to opening waves of the type proposed by Brune and co-workers involving dynamic stress reduction. The pulse can be compared to a propagating "dislocation" where asperities no longer intermesh, thus allowing slip to occur as illustrated schematically in Figure 15. It appears natural that such a disjunction between two rough surfaces, coupled with inertial effects, could lead to a propagating bulge that is similar to a ripple in a carpet being flicked across a floor. This picture could represent a possible mechanism for opening waves, should they exist.

A (weak) piece of evidence in support of the interface wave hypothesis is the form of particle trajectories during slip. Close to the fault, these are consistent with retrograde motion superimposed on the forward movement associated with slip (c.f. the trajectory of a point on a bicycle tire). In contrast, particle trajectories further away from the fault become pointed which is consistent with prograde motion superimposed with the forward movement. Consequently, the slip pulse may be

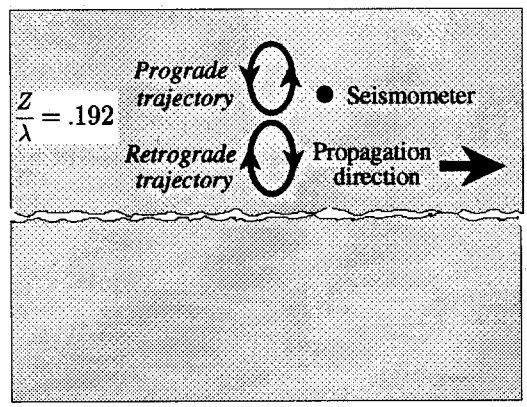

Figure 14
Rayleigh wave particle trajectories for a medium with Poisson's ratio of 0.25. The indicated seismometer will record prograde motion whereas a seismometer near the fault surface would record retrograde motion.

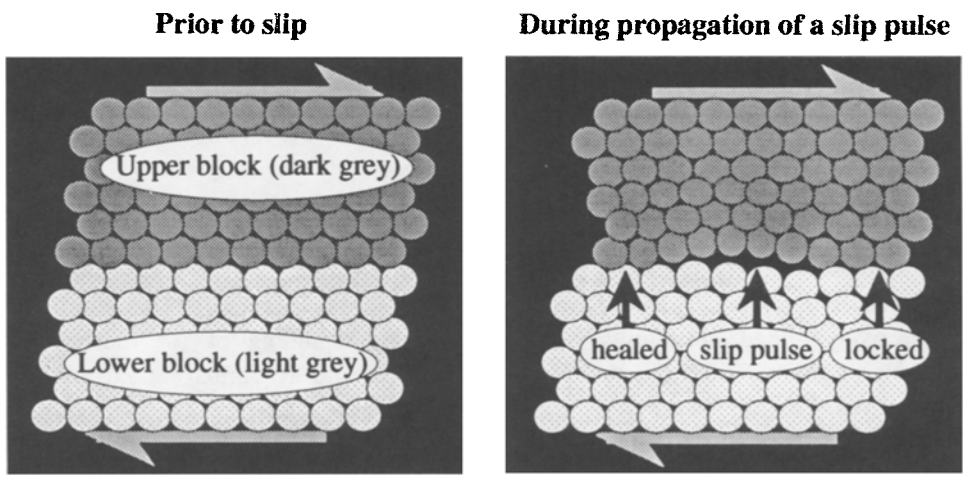

Figure 15
Schematic illustration of a possible mechanism for a propagating (self-healing) slip pulse. Healing after the pulse occurs due to matching of the dominant asperities (represented in the figure as the intermeshing of particle rows adjacent to the fault). Note that both rows adjacent to the fault are ten particle diameters wide but the upper row is compressed during the propagation of the self-healing slip pulse leading to a ripple in the upper block (right figure). Note that in the numerical experiment, the slip pulse was approximately 50 particle diameters wide and spanned several larger asperities (than the bumps on the particle rows shown above). The data recorded in the numerical experiment was insufficient to determine whether interface opening occurs as shown here or whether the normal motions were due entirely to surface roughness with particles remaining in contact within the slip zone.

carried by an interface wave with Rayleigh-like characteristics[9] (see Figure 14). This observation would only have relevance if Rayleigh motions could not be excited by a roughness induced slip pulse.

In view of the slip magnitudes of one particle diameter, there is not expected to be any intrinsic velocity weakening effect in the usual sense within the slip pulse despite the presence of global slick-slip behavior (i.e., the particle interactions are elastic). Velocity weakening would result if larger slip magnitudes were present due to the transfer of momentum from the in-plane to normal direction (LOMNITZ-ADLER, 1991) or in-plane interactions (PISARENKO and MORA, 1994). Consequently, the stick-slip behavior in the numerical experiment is entirely due to the unlocking and locking of the smallest asperities. Ideally, numerical experiments involving much larger systems of particles should be conducted in order to study the behavior when a range of slip magnitudes are possible and to determine whether

[9] Rayleigh waves have retrograde particle motions near the free surface and prograde particle motions beyond a certain distance from the surface (0.192 times the wavelength of Rayleigh waves for a medium with Poisson's ratio of 0.25).

the slip pulses can be induced by a more realistic surface roughness. This will be the subject of future research using the lattice solid model.

Comment

The lattice solid model offers two main possibilities:
(1) studies involving *simplified* particle interactions, and
(2) studies involving *realistic* particle interactions,
respectively aimed at gaining an improved understanding of the mechanisms underlying the nonlinear dynamics of earthquakes and at simulating earthquakes themselves. The numerical study presented in this paper falls into the *first category* and involves the simplest particle interactions imaginable. Despite the limited size of the model and simplicity of the interactions, stick-slip behavior was observed with considerable similarity to that observed in physical experiments and the field. For this reason, we are confident that the second possibility is real, at least in principle. In practice, this would require substantially larger systems of particles to be simulated (e.g., 10^9-10^{12} particles) which may become feasible in the near future considering the current rate of increase in computer speeds (a factor of approximately 2 every 1.5 years). Perhaps a more fundamental requirement is the specification of "realistic" particle interactions. This is not a simple matter of incorporating knowledge gained through rock physical experiments. For example, the dynamical friction between rock surfaces at seismic slip rates has not been measured in laboratory experiments. However, we hope that sufficiently realistic interactions can be obtained in the future through physical experimentation involving improved laboratory techniques coupled with numerical studies using "microscopically" based approaches such as the lattice solid model and related spring-asperity model (PISARENKO and MORA, 1994).

Conclusions

Realistic frictional behavior has been simulated by modeling a 2D system of particles representing frictionless circular grains linked by elastic-brittle bonds. Stick-slip events are observed in a numerical experiment involving two blocks with rough surfaces being rubbed past one another at a constant rate. The stick-slip behavior is entirely due to the surface roughness coupled with the elastic stiffness of blocks considering there is no friction between particles. A slip pulse initiates when the shear stress is sufficient to push two interlocking asperities past one another. The pulse fronts propagate along the fault at speeds ranging between the Rayleigh wave speed and a value somewhat higher than the shear wave speed in agreement with theory and observation. Slip rates comparable to generally accepted values

have been observed in the initial part of a slip pulse whose front propagates at the Rayleigh wave speed. Within the main part of the pulses, the slip rates are an order of magnitude higher, possibly due to the combined effect of the lack of friction between particles and the high driving plate velocities, or alternatively, uncertainties in the estimates based on seismogram inversion. Particle trajectories indicate that slip occurs as the blocks locally jump apart. The form of the trajectories is similar to those observed by BRUNE *et al.* (1993) which lead them to suggest that interface (opening) waves may exist that could explain the heat flow paradox. However, it is not yet clear whether the normal motions observed in the numerical experiment are a consequence of surface roughness alone or whether they relate to such interface waves. Future work is required to address this issue, to refine the lattice solid model and to conduct experiments with larger systems of particles that will allow realistic surface roughness to be specified.

Acknowledgements

P. M. would like to thank: Paul Davis for encouragement and drawing attention to the work of Brune and co-workers; Jim Brune and Chris Archer for rapidly providing preprints; Pascal Bernard for sharing his knowledge of seismogram spectra; Steve Brown and an anonymous reviewer for helpful comments; Chris Marone for serious and constructive editing and review comments; Dmitri Pisarenko for useful insights and references; Frédéric Donzé for stimulating discussion.

Computations were performed at the Centre National de Calcul Parallèle en Sciences de la Terre in France and funded by the French Ministry of Education and Research. This research has been funded in part by the French National Center for Scientific Research (CNRS) and the Sponsors of the Seismic Simulation Project (Amoco, CEA [French Atomic Energy Authority], Onyx Sciences Corp., Elf Aquitaine, GOCAD, Norsk Hydro, Shell, Thinking Machines Co., Total).

Special thanks to Hubert Delany, author of the CRYSTAL 3D graphics package.

REFERENCES

AKI, K., and RICHARDS, P. G., *Quantitative Seismology: Theory and Methods* (Freeman and Co., San Francisco 1980).

ALLEN, M. P., and TILDESLEY, D. J., *Computer Simulations of Liquids* (Oxford Univ. Press, New York 1987).

ANDREWS, D. J. (1976), *Dynamic Plain Strain Shear Rupture with a Slip Weakening Friction Law Calculated by the Boundary Integral Method*, Bull. Seismol. Soc. Am. *75*, 1–21.

ARCHULETA, R. J. (1982), *Analysis of Near Source Static and Dynamic Measurements from the 1979 Imperial Valley Earthquake*, Bull. Seismol. Soc. Am. *72*, 1927–1956.

ASHURST, W. T., and HOOVER, W. G. (1976), *Microscopic Fracture Studies in the Two-dimensional Triangular Lattice*, Phys. Rev. B *14*, 1465–1473.

BAKUN, W. H., and MCEVILLY, T. V. (1984), *Recurrence Models and Parkfield, California, Earthquakes*, J. Geophys. Res. *89*, 3051–3058.

BOWDEN, F. P., and TABOR, D. (1950), *The Friction and Lubrication of Solids* (Clarendon Press, Oxford 1950).

BROWN, S. R., and SCHOLZ, C. H. (1985), *Broad Bandwidth Study of the Topography of Natural Rock Surfaces*, J. Geophys. Res. *90*, 12,575–12,582.

BRUNE, J. N., JOHNSON, P. A., and SLATER, C. (1990), *Nucleation, Predictability, and Rupture Mechanism in Foam Rubber Models of Earthquakes*, J. Himalayan Geol. *1*, 155–166.

BRUNE, J. N., BROWN, S., and JOHNSON, P. A. (1993), *Rupture Mechanism and Interface Separation in Foam Rubber Models of Earthquakes: A Possible Solution to the Heat Flow Paradox and the Paradox of Large Ovethrusts*, Tectonophys. *218*, 59–67.

BURRIDGE, R., CONN, G., and FREUND, L. B., (1979), *The Stability of a Plain Strain Shear Crack with Finite Cohesive Force Running at Intersonic Speeds*, J. Geophys. Res. *84*, 2210–2222.

BURRIDGE, R., and KNOPOFF, L. (1967), *Model and Theoretical Seismicity*, Bull. Seismol. Soc. Am. *57*, 341–371.

BYERLEE, J. D., and BRACE, W. F. (1968), *Stick Slip, Stable Sliding, and Earthquakes – Effect of Rock Type, Pressure, Strain Rate, and Stiffness*, J. Geophys. Res. *73*, 6031–6037.

CARLSON, J. M., and LANGER, J. S. (1989), *Mechanical Model of an Earthquake Fault*, Phys. Rev. A *40*, 6470–6484.

CHRIST, N. H., FRIEDBERG, R., and LEE, T. D. (1982), *Random Lattice Field Theory*, Nucl. Phys. B *202*, 89–125.

COCHARD, A., and MARADIAGA, R. (1993), *Dynamic Faulting under Rate-dependent Friction*, Pure and Appl. Geophys. *142*, 419–445.

COMNINOU, M., and DUNDURS, J. (1977), *Elastic Interface Waves Involving Separation*, J. Appl Mech. *44*, 222–226.

COMNINOU, M., and DUNDURS, J. (1978), *Elastic Interface Waves and Sliding between Two Solids*, J. Appl. Mech. *45*, 325–330.

DAY, S. M. (1991), *Numerical Simulation of Fault Propagation with Interface Separation*, AGU 1991 fall mtg. Prog. and abstracts, published as supp. to EOS, Oct. 29, 1991.

DIETERICH, J. H. (1978), *Preseismic Fault Slip and Earthquake Prediction*, J. Geophys. Res. *83*, 3940–3948.

DONZÉ, F., MORA, P., and MAGNIER, S. A. (1993), *Numerical Simulation of Faults and Shear Zones*, Geophys. J. Int. *116*, 46–52.

FREUND, L. B. (1978), *Discussion*, J. Appl. Mech. *45*, 226–228.

FREUND, L. B., *Dynamic Fracture Mechanics* (Cambridge Univ. Press, Cambridge 1990).

HEATON, T. H. (1990), *Evidence for and Implications of Self-healing Pulses of Slip in Earthquake Rupture*, Phys. Earth Planetary Interiors. *64*, 1–20.

HEATON, T. H. (1994), *pers. comm.*

HESLOT, F., BAUMBERGER, T., PERRIN, B., CAROLI, B., and CAROLI, C. (1994), *Creep, Stick-slip and Dry Friction Dynamics: Experiments and Heuristic Model*, Phys. Rev. *submitted.*

HERRMANN, H. J. (1993), *pers. comm.*

HOOVER, W. G., ASHURST, W. T., and OLNESS, R. J. (1974), *Two-dimensional Computer Studies of Crystal Stability and Fluid Viscosity*, J. Chem. Phys. *60*, 4,043–4,047.

LOMDAHL, P. S., TOMAYO, P., GRØNBECH-JENSEN, N., and BEAZLEY, D. M., *50 Gflops molecular dynamics on the Connection Machine 5.* In *Proc. SuperComputing 93, Portland Oregon, Nov. 15–19* (IEEE Computer Soc. Press 1993a).

LOMDAHL, P. S., BEAZLEY, D. M., TOMAYO, P., and GRØNBECH-JENSEN, N. (1993b), *Multi-million Particle Molecular Dynamics on the CM-5*, Int. J. Mod. Phys. C *4*, 1075–1084.

LOMNITZ-ADLER, J. (1991), *Model for Steady State Friction*, J. Geophys. Res. *96*, 6121–6131.

MORA, P., and PLACE, D. (1993), *A Lattice Solid Model for the Nonlinear Dynamics of Earthquakes*, Int. J. Mod. Phys. C *4*, 1059–1074.

NIELSEN, S. B., and TARANTOLA, A. (1992), *Numerical Model of Seismic Rupture*, J. Geophys. Res. *97*, 15,291–15,295.

PISARENKO, D., and MORA, P. (1994), *Velocity Weakening in a Dynamical Model of Friction*, Pure and Appl. Geophys. *142*, 447–466.

RICE, J. R. (1993), *Spatio-temporal Complexity of Slip on a Fault*, J. Geophys. Res. *98*, 9885–9907.

SCHALLAMACH, A. (1971), *How Does Rubber Slide?*, Wear *17*, 301–312.

SCHOLZ, C. H., *The Mechanics of Earthquakes and Faulting* (Cambridge Univ. Press., Cambridge 1990).

SCHOLZ, C., MOLNAR, P., and JOHNSON, T. (1972), *Detailed Studies of Frictional Sliding of Granite and Implications for Earthquake Mechanism*, J. Geophys. Res. *77*, 6392–6406.

SCHROEDER, M., *Fractals, Chaos, Power Laws* (Freeman, New York 1991), p. 122.

(Received September 9, 1993, revised April 2, 1994, accepted April 25, 1994)